# Polymeric microneedle-mediated transdermal delivery of melittin for rheumatoid arthritis treatment

Du, Guangsheng ; He, Penghui; Zhao, Jiaxuan; He, Chunting; Zhang, Zhihua; Zhang, Zhibing; Sun, Xun

*DOI:*
10.1016/j.jconrel.2021.07.005



*Document Version*
Peer reviewed version

*Citation for published version (Harvard):*
Du, G, He, P, Zhao, J, He, C, Zhang, Z, Zhang, Z & Sun, X 2021, 'Polymeric microneedle-mediated transdermal delivery of melittin for rheumatoid arthritis treatment', *Journal of Controlled Release*, vol. 336, pp. 537-548. https://doi.org/10.1016/j.jconrel.2021.07.005

# Polymeric microneedle-mediated transdermal delivery of melittin for rheumatoid arthritis treatment

Guangsheng Du[1], Penghui He[1], Jiaxuan Zhao[1], Chunting He[1], Min Jiang[1], Zhihua Zhang[2], Zhibing Zhang[2], Xun Sun[1]*

[1] Key Laboratory of Drug-Targeting and Drug Delivery System of the Education Ministry, Sichuan Engineering Laboratory for Plant-Sourced Drug and Sichuan Research Center for Drug Precision Industrial Technology, West China School of Pharmacy, Sichuan University, Chengdu, 610064, PR China

[2] School of Chemical Engineering, University of Birmingham, Edgbaston, Birmingham, B15 2TT, UK

*Corresponding author

E-mail address: sunxun@scu.edu.cn

**Abstract**

Transdermal drug delivery systems for rheumatoid arthritis (RA) have been receiving increasing attention as they can potentially overcome drawbacks which exist in traditional oral or injection strategies, including low patient compliance and serious gastrointestinal side effects. However, transdermal delivery of RA drugs especially biological drugs suffers from low drug delivery efficiency due to the robust skin barrier. Herein, we fabricated melittin-loaded hyaluronic acid (HA) microneedles and investigated their capacity for inhibiting RA. We showed that melittin-loaded HA microneedles possessed high mechanical strength for successful delivery of melittin into the skin and effectively inhibited RA progression in adjuvant induced both rodent and murine models, as shown by results in histological, paw swelling and arthritis score. Furthermore, after modifying HA with cross-linkable groups, the fabricated microneedles with sustained release properties could further improve the therapeutic potency. Cytokine and T cell analysis in the paws and lymphatic organs indicated that the application of microneedles suppressed the levels of pro-inflammation cytokines including IL-17 and TNF-α, and increased the percentage of regulatory CD4 T cells. Our study revealed that polymeric microneedle-mediated transdermal delivery of melittin could serve as a new therapy with high compliance and good therapeutic efficacy for RA and other autoimmune diseases.

**Keywords:** Polymeric microneedles; Melittin; Rheumatoid arthritis; Sustained release; Hyaluronic acid

## Introduction

Rheumatoid arthritis (RA) is an autoimmune disease that is characterized by chronic synovial inflammation. It affects about 1% of the adult all over the world and can cause serious damage of cartilage and bone, and finally lead to disability [1]. Currently, RA is normally treated by oral administration or injection of non-steroidal anti-inflammatory drugs (NSAIDs) or corticosteroids [2]. These strategies can decrease inflammation and retard the progression of RA by interfering with inflammation related pathways, for example by decreasing the levels of pro-inflammatory cytokines, inhibiting cell-mediated immune responses, or suppressing synovial collagenase gene expression [3, 4]. However, these traditional strategies suffer from low patient compliance due to the pain or infection caused by the injection or the serious gastrointestinal side effects observed after frequent oral administration. Additionally, the harsh gastrointestinal environment and liver first-pass effect could result in a significantly low drug bioavailability [5].

As an attractive alternative, transdermal delivery systems for RA have been receiving increasing attention [6]. Transdermal delivery of RA drugs could avoid gastrointestinal digestion in oral route and pain sensation caused by injection. Furthermore, the easiness for self-administration further increases their attractiveness. Small-molecule drugs formulated in transdermal patch or gel have been shown to diffuse into the skin and exhibit anti-RA effect [7, 8]. However, the passive diffusion of drug is significantly limited by the robust skin barrier, and has strict requirements on the properties of applied drugs, including log p-value of 1-3, molecular weight below 500 Da and appropriate amount of H-bond donors and acceptors [6]. Besides, penetration enhancers and nanoparticle technology have been utilized to improve drug delivery efficiency through the skin [9-11]. Nevertheless, transdermal delivery of biological drugs in a therapeutically relevant amount is still challenging due to their often large molecular weight and high hydrophilicity [12].

Polymeric microneedles are micro-structured needles with a length of 200-1000 μm. They can overcome the skin barrier in a non-invasive and pain-free way as they are long enough to penetrate the skin but short enough not to touch the nerves and blood vessels [13, 14]. Compared to traditional transdermal gel or patch, microneedles can significantly increase transdermal delivery efficiency of biological drugs such as protein and peptide drugs [15]. Additionally, polymeric microneedles do not result in any hazardous waste after administration and the easiness for polymer functionalization allows possibilities to modulate release properties of the loaded drugs. Hyaluronic acid (HA) is one of the mostly used polymers for fabrication of polymeric microneedles and can dissolve within minutes after being inserted into the skin. After modifying HA with functional groups, the obtained microneedles can be endowed with controlled release properties of the loaded drugs, which have been shown to increase therapeutic efficacy of the microneedles [16, 17].

As compared to metal or silicone microneedles, polymeric microneedles possess relatively much lower mechanical strength, which may cause insufficient penetration of the skin and result in low drug delivery efficiency [18, 19]. In previous studies, researchers have characterized the mechanical strength of polymeric microneedles by compressing the whole patch with a flat surface and calculating the rupture force of single microneedles by dividing the rupture force of the patch by the number of microneedles

[19, 20]. However, this method is not adequate since it can not give possible variations among the microneedles within the patch, and the calculated mechanical property parameter is limited to rupture force. In our lab, we have applied a micromanipulation technique to precisely characterize the mechanical properties of individual microneedles. We have observed that as compared to rupture force, rupture stress is a better indicator for the mechanical strength of the microneedles [21, 22].

Previous studies including several clinical trials conducted in East Asia have indicated that bee venom acupuncture exerted anti-inflammation efficacy with minimum side effects in arthritis diseases [23]. Further studies revealed that the water-soluble fractions of bee venom can establish anti-inflammatory effect and reduce disease progression in RA [24, 25]. It turned out that melittin, a cationic peptide containing 26 nucleic acids, is the main component in bee venom for immune modulation and anti-RA effects [26]. However, the use of live bees or injection of purified melittin could cause significant pain and melittin itself has also a risk for causing serious hemolysis after intravenous injection [27]. These drawbacks have significantly limited the therapeutic application of melittin for RA. Transdermal delivery of melittin, for example by using microneedles, could potentially overcome the drawbacks mentioned above. So far, to our best knowledge, there has been no report on the delivery of melittin by using microneedles.

In the current study, we propose to develop melittin-loaded polymeric microneedles for the treatment of RA, aiming for increasing patient compliance and therapeutic potency. The scheme is shown in Figure 1. Melittin was loaded into HA based microneedles and the mechanical strength of individual microneedles was characterized by micromanipulation. The therapeutic potency of the fabricated microneedles to treat RA was investigated in both rodent and murine AIA models. We showed that although the loading of melittin decreased the mechanical strength of the microneedles, the drug loaded in the microneedles was successfully delivered into the skin and significantly inhibited the progression of RA by reducing excretion of pro-inflammatory cytokines and by altering cellular immunity. We also observed that after modifying HA with methacrylate groups, the obtained microneedles with sustained release properties could further increase therapeutic efficacy. Our study suggested that polymeric microneedles for transdermal delivery of biological drugs could be a promising RA treatment strategy for improving patient compliance and therapeutic potency.

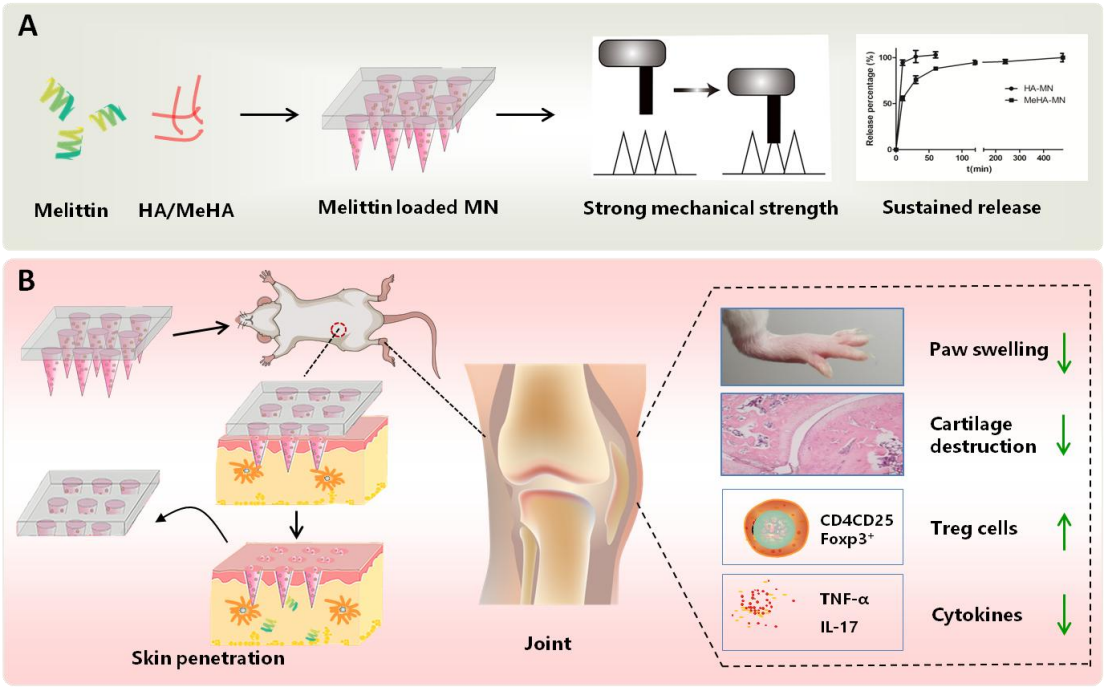


**Figure 1**. Scheme of microneedle-mediated delivery of melittin for RA treatment. A: Fabrication of microneedles and characterization of mechanical strength and release behavior. B: The fabricated microneedles successfully delivered melittin into the skin and inhibited RA progression, as shown by results in histological, paw swelling, and levels of pro-inflammatory cytokines and Treg cells. HA: hyaluronic acid, MN: microneedles, MeHA: methacrylate modified hyaluronic acid, Treg: CD4 regulatory T cells.

## 2 Materials and methods

### 2.1 Materials

HA with a molecular weight of 10,000 Da was obtained from Bloomage Biotechnology (Jinan, China). Melittin (≥96%) with an amino acid sequence of GIGAVLKVLTTGLPALISWIKRKRQQ-NH2 was obtained from GL Biochem Ltd. (Shanghai, China). SYLGARD$^{TM}$ 184 silicone elastomer containing both base and curing agent was purchased from DOWSIL (MI, US). Fluorescein isothiocyanate (FITC) and Cy5 dye were purchased from Meilunbio (Dalian, China). Methacrylic anhydride (MA), N'-methylenebisacrylamide (MBA), Irgacure 2959 and NaOH were purchased from Sigma Aldrich (Shanghai, China). 4% paraformaldehyde was obtained from Leagene Biotechnology (Beijing, China). Anhydrous silica gel was purchased from Chron Chemicals (Chengdu, China). Antibodies for CD3, CD4, CD25, Foxp3, and Elisa kits for TNF-α and IL-17 were obtained from Invivogen (Toulouse, France). Optimal cutting temperature compound (OCT) medium was purchased from Sakura (Shanghai, China). Milli Q water (18 MΩ/cm, Millipore Co.) was used for the preparations of all solutions. All other reagents used were of analytical grade and used as received.

### 2.2 Synthesis of methacrylate modified hyaluronic acid (MeHA)

MeHA was synthesized by modifying HA with methacrylate groups as previously described [28]. Briefly, 5 g of HA was added into 100 mL water and incubated overnight for complete dissolution. 8 mL MA was subsequently added into HA solution and pH of the solution was adjusted to 8. The mixture was then stirred at 4 °C and incubated for overnight. Afterwards, the obtained MeHA was precipitated by acetone, washed by ethanol for 3 times and dialyzed against water for 48 h to remove excess MA. Finally, the purified MeHA was dried in an ice condenser (Labconco FreeZone 2.5, Hampton, VA) in freeze vacuum (-50 °C, 90 mbar) overnight, and stored in dry environment for further use and analysis.

To verify if the chemical modification was successful, the $^{1}$H nuclear magnetic resonance ($^{1}$H NMR) spectrum of the obtained MeHA was characterized by using a Bruker 400 MHz NMR spectrometer (Bruker, Switzerland) in $CDCl_3$.

### 2.3 Fabrication of melittin loaded microneedles

HA-based microneedles were fabricated by using a micro-molding method. Briefly, a stainless steel microneedle patch, which contains 10×10 needles with a needle length of 700 μm and base to base length of 300 μm on a plate of 0.9×0.9 $cm^2$, was first used to make polydimethylsiloxane (PDMS) mold. The metal microneedle patch was immersed in SYLGARD$^{TM}$ 184 silicone elastomer containing base and curing agent with a volume ratio of 10:1, and the mixed agent was cured by heating at 90 °C for 2 h. Next, the metal microneedle patch was peeled off and the obtained PDMS mold was used for fabrication of the microneedles.

To prepare melittin loaded HA microneedles (Mel-HA-MN), appropriate amount of melittin was first dissolved into 1 mL of 500 mg/ml HA solution. Next, 30 μL of the matrix solution was filled into the PDMS mold using pressurized air at 0.2 MPa for 3 min. After removing the excess matrix solution, the matrix in the mold was dried in a glass dessicator containing anhydrous silica gel for 1 h. In the next step, 40 μL of HA solution (500 mg/mL) was added into the mold to prepare back-plate of the patch. The mold was dried in the anhydrous silica gel environment for another 4 h. Finally, the microneedle patch was peeled off from the PDMS mold and stored for further use and analysis. To fabricate melittin loaded MeHA microneedles (Mel-MeHA-MN), 30 μL of polymer solution consisting appropriate amount of melittin, 40 mg/mL MeHA, 20 mg/mL MBA and 0.5 mg/mL photo-initiator Irgacure 2959 was first filled into the PDMS mold by pressurized air as mentioned above. The matrix in PDMS mold was dried in anhydrous silica gel environment for 1 h, and 60 μL of blank HA solution (500 mg/mL) was further added to fabricate the back-plate. The rest of the procedures were the same as that for fabrication of Mel-HA-MN. Finally, the dried microneedle patch was cross-linked by ultraviolet radiation at 365 nm for 15 s. The fabricated microneedle patches contain either 15 μg or 100 μg melittin per patch, which were used for mice and rat study, respectively. To fabricate melittin-loaded microneedles for visualization by confocal laser scanning microscopy (CLSM), FITC or Cy5 labelled melittin was used for the fabrication of microneedles. To obtain FITC- or Cy5-labelled melittin, melittin was incubated with FITC or Cy5 dye for 1 h, and the excess free dye was removed using a dialysis bag with a cut-off of 2,000 Da.

### 2.4 Visualization of microneedles

Surface morphology of the fabricated microneedles was characterized by both scanning electronic microscopy (SEM) and CLSM. For SEM visualization, the microneedles were coated with a thin layer of carbon and visualized with a voltage of 15.0 KV by using a FEI Nova NanoSEM (Eindhoven, The Netherlands). For visualization by CLSM, the microneedles were scanned with a step speed of 5 μm/step by using a 10× Plan Apo objective.

2.5 Characterization of mechanical properties of individual microneedles

The mechanical properties including rupture behavior of individual microneedles were characterized by using micromanipulation as previously reported [21]. Briefly, individual microneedles were put between the sample stage of the micromanipulation instrument and an optical glass rod made of Borosilicate with a diameter of 100 μm as a sensor of a force transducer (Model GSO-10, Transducer Techniques, LLC, USA). Single microneedles were compressed between the stage and the glass probe with a compression speed of 2 μm/s. The curve of compression force versus microneedle deformation was recorded. With this information as well as mathematic modeling, rupture displacement and rupture stress of individual microneedles were obtained, which has been described with details in a previous study [21]. The compression process is shown in Supplementary video. For each type of patch, 30 microneedles were analyzed.

2.6 In vitro release behaviors of HA-based microneedles

To study in vitro release behavior of the microneedles, each patch was suspended in 1 mL PBS and shaken in a Bluepard shaker (Shanghai, China) with a speed of 100 rpm at 37 °C. At different time points (0, 10, 30, 60, 120, 240 and 480 min), 100 μL of the solution was withdrawn for analysis and the same volume of fresh PBS was added back. The concentration of melittin in the release solution was analyzed by a high-performance liquid chromatography (HPLC) (Agilent1260 Infinity, CA, USA) equipped with a Diamonsil C18 column (Dikma, Beijing, China). The mobile phase includes 0.1% trifluoroacetic acid (TFA) in water (solvent A) and 0.1% TFA in acetonitrile (solvent B). The composition of mobile phase changes from 95% solvent A/5% solvent B to 5% solvent A/95% solvent B within 25 min. The absorbance was detected at 220 nm. The concentration of melittin was calculated by using a calibration curve ($y=2.5819x+2.6778$, $R^2=0.9998$).

2.7 Animals used in this studyMale BALB/c mice of 6-8 weeks old (body weight 18-20 g) and male Sprague Dawley (SD) rats of 6-8 weeks old (body weight 180-200 g) were purchased from Dashuo Biotechnology Company (Chengdu, China). All animal experiments were performed following guidelines approved by the ethics committee of Sichuan University. The animals were housed under standardized conditions in the animal facility.

2.8 Penetration capacity of the fabricated microneedles in animal skin

The penetration capacity of fabricated microneedles was evaluated by Trypan blue staining method. Briefly, the microneedles loaded with melittin were applied manually onto the skin. After 1 min, the microneedle patch was removed and the penetrated skin was stained with 200 μL 4% Trypan blue for 2 min. After removing the excess dye and washing with water for 3 times, the stained skin was visualized

by bright field microscopy. To evaluate the penetration depth, microneedles loaded with FITC labeled melittin were applied onto the skin. After 3 min, the back-plate of microneedles was removed and the penetrated skin was excised, embedded in optimal cutting temperature compound (OCT) medium and sectioned by using a Leica CM 1950 freezing microtome (Buffalo Grove, IL). Next, the inserted microneedle tips in the skin specimens were visualized by a 10× Plan Apo objective.

2.9 In vivo release and biodistribution of melittin from Mel-MeHA-MN

The in vivo release behavior of melittin from Mel-MeHA-MN was evaluated in BALB/c mice skin. MeHA microneedles loaded with Cy5 labelled melittin or free Cy5 were penetrated into mice abdomen skin as described above. Afterwards, the fluorescence in the animal skin was visualized by using a PerkinElmer in vivo imager (Shanghai, China) at different time points. The animals were monitored at day 1, 2, 3, 4, 6 and 7.

To investigate the biodistribution of melittin, Cy5-labelled melittin was given to BALB/c mice by either S.C. injection or Mel-MeHA-MN. At 8 h after administration, the mice were sacrificed and tissues including heart, liver, spleen, lung, kidney, joint and blood were isolated for visualization by the in vivo imager. Blood containing 10 μg/ml melittin was used as a control.

2.10 Therapeutic potency of Mel-HA-MN in adjuvant-induced arthritis (AIA) rodent model

To build rat AIA model, SD rats were injected into each of hint foot pad with 80 μL complete Freund's adjuvant which contains 10 mg/mL Mycobacterium tuberculosis on day 0. From day 4 when early arthritis was established, the animals were treated by Mel-HA-MN loaded with 100 μg melittin or by subcutaneous (S.C.) injection of the same dose on abdomen skin every other day for 8 times (n=6). The doses were selected by referring to previous studies [29, 30]. AIA rats without any treatment were used as a control. On day 22, the animals were sacrificed and paws and blood were collected for further analysis.

During the treatment, the weight of animals was recorded to calculate the percentage of the weight loss compared to the base. The thickness of two hind paws was measured using a vernier caliper every other day to calculate the average change of ankle thickness. The clinical symptoms were scored at a scale of 0-4 (0, no erythema or swelling; 1, mild erythema and swelling confined to ankle joint; 2, mild erythema and swelling extending from the ankle to the tarsals; 3, moderate erythema and swelling extending to metatarsal joints; 4, pronounced erythema and swelling of entire paw).

The blood on day 22 was withdrawn to study the hematologic parameters including counts of white blood cells (WBC), red blood cells (RBC) and platelets. Analysis was performed on a Mindray BC-2800 Vet (Shenzhen, China).

For histological examination, the collected paws were first fixed in 4% paraformaldehyde for 24 h. The fixed paws were immersed in saturated EDTA-2Na solution and shaken in a Bluepard shaker (Shanghai, China) with a speed of 180 rpm for 2 month for decalcification of the paws. The saturated EDTA-2Na solution was refreshed every week until the decalcification was complete. Next, the paws were

embedded in paraffin, sectioned at 5 μm and stained with haematoxylin and eosin (H&E) or Safranin O-fast green. The inflammatory cell influx and cartilage integrity were assessed.

2.11 Therapeutic potency of Mel-MeHA-MN in murine AIA model

Mouse AIA model was induced by injection of 20 μL complete Freund's adjuvant which contains 10 mg/mL Mycobacterium tuberculosis into each of the hind foot on day 0. Starting from day 4, when the early arthritis was established, male BALB/c mice of 6-8 weeks old were treated with the following groups: 15 μg melittin loaded Mel-MeHA-MN, 15 μg melittin loaded Mel-HA-MN and S.C. injection of 15 μg melittin. AIA mice receiving no treatment were used as a control. The various formulations were administered every other day for 6 times. On day 16, mice were sacrificed and blood, hind paws, spleen and popliteal lymph nodes were collected for further analysis. The animal weight loss, hind paw thickness change and arthritic scores were monitored using the same method as described for the therapeutic potency study in AIA rodent model.

Pro-inflammation cytokines including TNF-α and IL-17 in the serum and paws were measured using ELISA kits according to the manufacturer's instructions. Serum was obtained by centrifuging the collected blood at 2000 g for 10 min with a Sigma 3K15 (Shanghai, China). The collected paws were cut into small pieces, suspended in PBS to reach a mass concentration of 1 g/mL and processed with glass homogenizers. The obtained suspension was centrifuged at 2500 g for 10 min to obtain the supernatant. To measure the cytokine concentrations, 100 μL of capture antibody in coating buffer was added into each well of 96 well-plates and incubated at 4 °C for overnight. After washing the wells with 300 μL buffer for 3 times, 200 μL of block buffer was added into each well and incubated for 1 h at room temperature. The plates were washed and 100 μL of standards or samples was added into each well and incubated for another 2 h at 4 °C. Next, 100 μL of detecting antibody was added into each well and incubated at room temperature for 1 h. The plates were washed again for 4 times and 100 μL of diluted Horseradish peroxidase conjugate (HRP) was added into each well and incubated for 30 min at room temperature. Subsequently, 100 μL of tetramethylbenzidine (TMB) solution was added into each well and incubated for 15 min. Finally, the reaction was stopped by adding 150 μL of 2 M sulfuric acid and the absorbance was measured at 450 nm with a Tecan Spark 10M plate reader (Männedorf, Switzerland).

The blood on day 16 was withdrawn to study the hematologic parameters as described in the last section, including WBC, RBC, platelets and percentage of lymphocytes, monocytes and granulocytes in WBC. H&E stain analysis was performed according to the same procedure as described in the therapeutic potency study of AIA mouse model.

Percentage of CD4 T regulatory cells (Treg) in spleen and popliteal lymph nodes were measured by flow cytometry (Cytomics FC 500, Beckman, Indianapolis, IN, USA). Briefly, single cell suspensions were obtained by forcing the spleen and popliteal lymph node through 70 μm strainers. The cells were centrifuged at 500 g for 5 min and washed with PBS for two times. Subsequently, the cells were resuspended in PBS and 200 μL of the cells was transferred to each well of 96-well plates. 100 μL of diluted surface staining antibodies including APC conjugated anti-CD3, APC-Cy7 conjugated CD4 and FITC

conjugated CD25 were added into each well and incubated for 30 min in the dark at 4 °C. After washing with FACs buffer, the cells were resuspended in freshly prepared fixation/permeabilization solution and incubated for 30 min at 4 °C. The cells were then washed with the permeabilization buffer and resuspended in diluted PE-conjugated anti-Foxp3 antibody solution for 30 min. Finally, the cells were washed with permeabilization buffer and the percentage of Treg cells ($CD3CD4CD25Foxp3^{+}$) was analyzed by the flow cytometry. The data were analyzed by using a FlowJo software.

2.12 Statistical analysis

All the data of immunization studies were analyzed by one way ANOVA with Turkey post-test by using GraphPad Prism (version 5.02). The significant levels were set at *p<0.05, **p<0.01 and ***p<0.001.

## 3. Results

### Fabrication of Mel-HA-MN and Mel-MeHA-HA

MeHA was obtained by modifying HA with methacrylate groups as shown in Figure 2a. The successful modification was indicated by $^{1}H$ NMR spectrum peaks at 5.6 ppm (a, 1H, $CH^{1}H=C(CH_3)CO$), 6.1 ppm (a, 1H, $CHH^{1}=C(CH_3)CO$), 1.85 ppm (b, 3H, $CH_2=C(CH_3)CO$) and 1.92 ppm (c, 3H, $NHCOCH_3$) (Figure 2B). Our results showed that the yield was around 80% and the modification degree was around 32% by comparing the area of peaks under 5.6 and 6.1 ppm to the peak area under 1.92 ppm. Mel-HA-MN and Mel-MeHA-MN were fabricated by using micro-molding with a process as shown in Figure 2C. The microneedle patches were fabricated by a two-step filling method to avoid waste of drug. Bright field and SEM Images of microneedles (Figure 2D-2G) showed that the fabricated microneedles had a regular rectangular pyramid shape with sharp tips. As compared to the blank HA microneedles (Figure 2D-2E), the loading of melittin did not significantly change the tip sharpness or surface morphology of the corresponding microneedles (Figure 2F-2G). CLSM images of HA microneedles loaded with FITC labeled melittin (Figure 2H) and MeHA microneedles loaded with Cy5 labelled melittin (Figure 2I) indicated that melittin was uniformly distributed in the microneedles. The surface morphology of microneedles shown by CLSM was consistent with that of SEM, further confirming that we have successfully fabricated melittin loaded HA and MeHA microneedles.

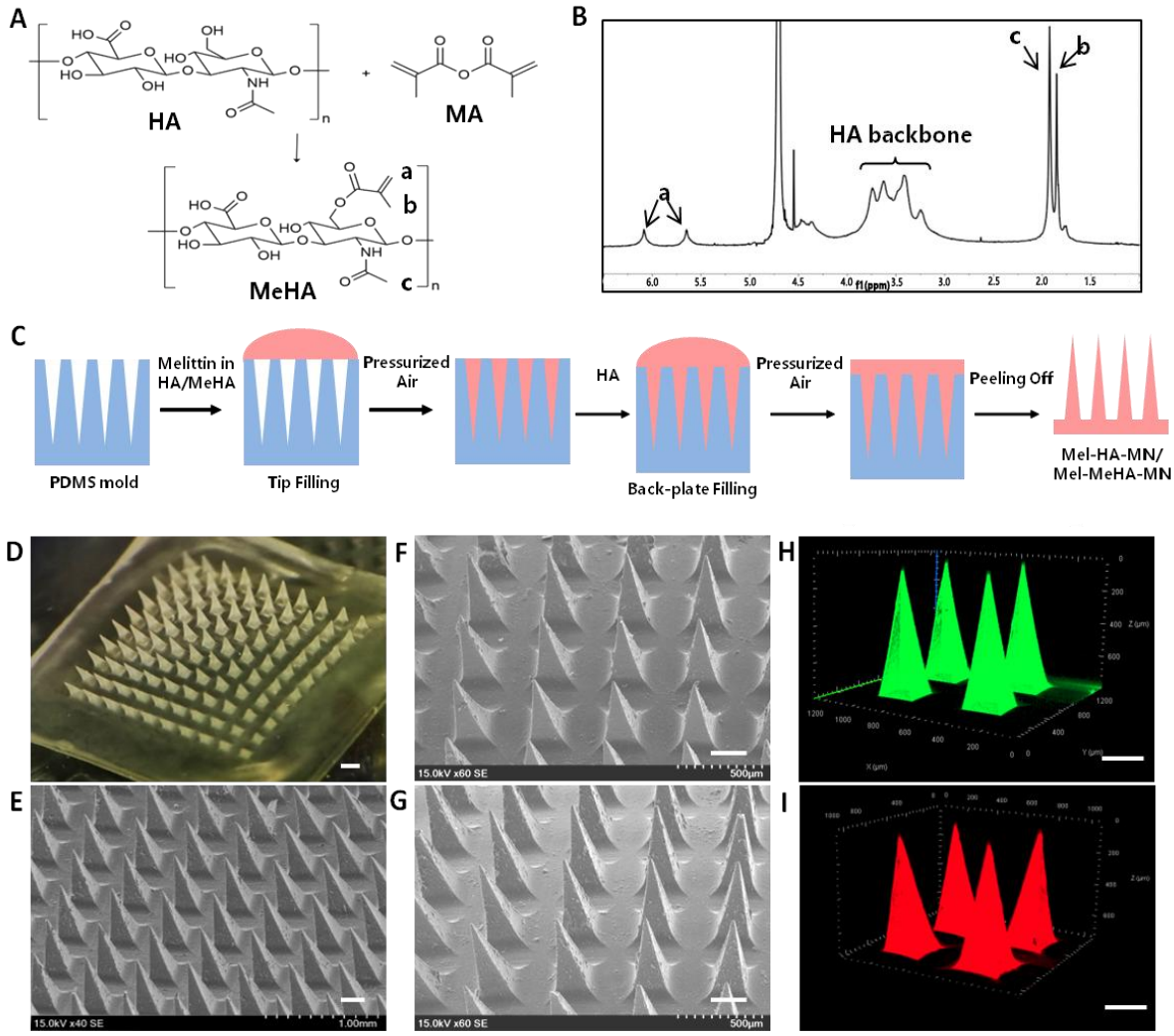


**Figure 2.** Fabrication and characterization of Mel-HA-MN and Mel-MeHA-MN. A: Synthesis of MeHA by modifying methacrylate groups on HA molecules. B: $^{1}$H NMR spectrum of MeHA indicated the successful modification of methacrylate groups on HA. C: Scheme of micro-molding method for fabrication of microneedles. D: Bright field image of blank microneedles. E-G: Scanning electronic microscopy (SEM) images of blank microneedles (E), Mel-HA-MN (F) and Mel-MeHA-MN (G). H: Confocal laser scanning microscopy (CLSM) image of HA microneedles loaded with FITC labelled melittin. I: CLSM image of MeHA microneedles loaded with Cy5 labelled melittin. Scale bar: 200 μm.

**Characterization of release behavior and biodistribution of melittin**

Next, we investigated and compared in vitro release behaviors of Mel-HA-MN and Mel-MeHA-HA in PBS. As shown in Figure 3A, all melittin was released from HA microneedles within 10 min. By contrast, Mel-MeHA-MN showed a burst release percentage of 56 % within 10 min and the rest of protein was sustainedly released until 480 min. The in vivo sustained release behavior of Mel-MeHA-MN was also evaluated in mice skin by using in vivo imager. Mel-MeHA-MN loaded with Cy5 labelled melittin was applied onto abdomen skin of BALB/c mice and the fluorescence of melittin was monitored on day 0, 2, 3, 4, 6 and 7. It was shown that the inserted microneedles remained in the skin and sustainedly released

melittin for 7 days, as shown by the slow elimination of fluorescence of melittin (Figure 3B). By contrast, the free Cy5 was eliminated within 3 days (Supplementary Figure 1).

The biodistribution of melittin was investigated by in vivo imager. As shown in Supplementary Figure 2, melittin was observed in liver, lung, kidney, joints and blood after both S.C. and microneedle application. Additionally, melittin level in the blood of the two treatment groups was much lower than the hemolytic concentration, as indicated by the much lower fluorescence intensity.

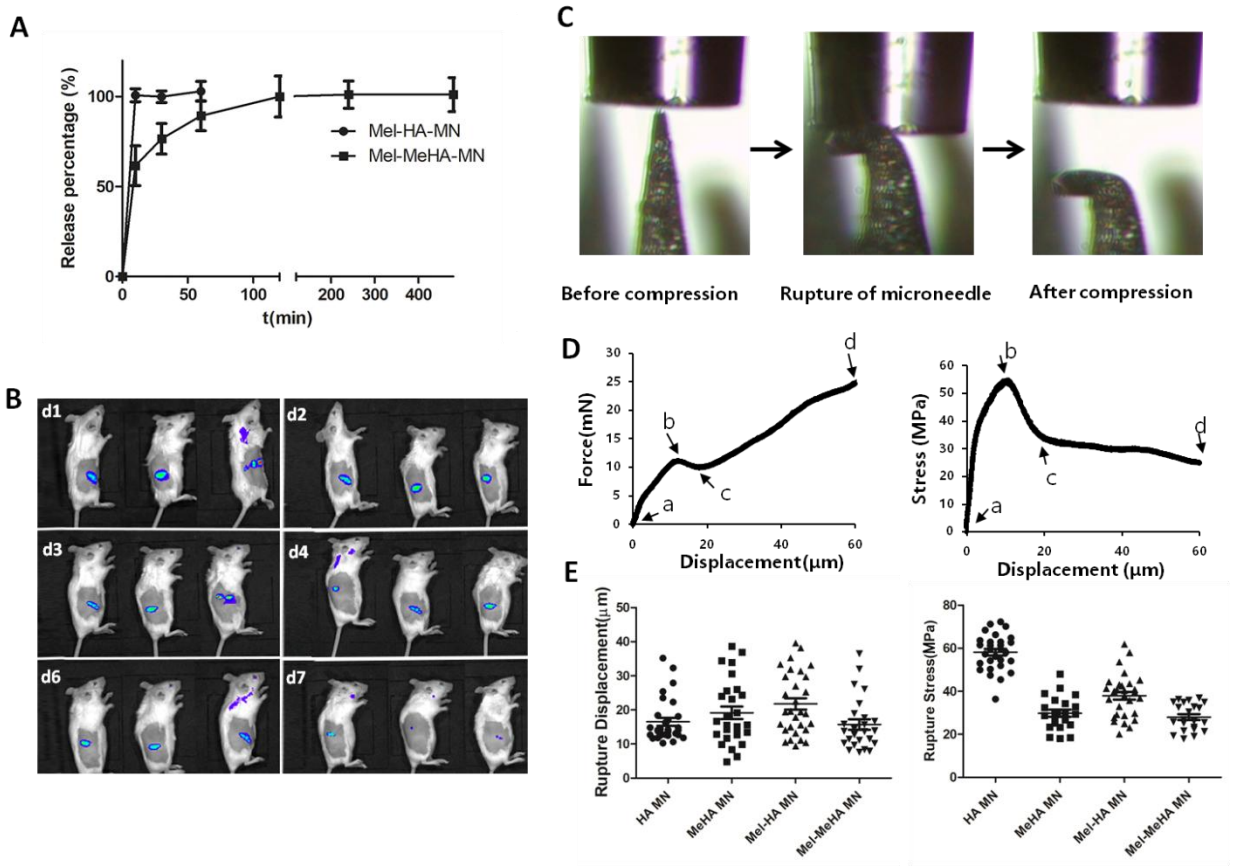


**Figure 3**. Release behavior and mechanical properties of the fabricated microneedles. A. In vitro release behaviors of Mel-HA-MN and Mel-MeHA-MN. B. In vivo release of Mel-MeHA-MN in BALB/c mice. C. Different status of single microneedles during compression by micromanipulation. D: Typical curves of rupture force and rupture stress versus microneedle displacement during compression. E: Rupture displacement and rupture stress of different microneedle patches.

**Characterization of mechanical strength of the fabricated microneedles**

Next, we evaluated the mechanical strength of individual microneedles by using micromanipulation. In Figure 3C, different status of microneedles during compression were shown, which are also reflected in Figure 3D. The microneedles were compressed at point a, and ruptured at point b where both rupture force and rupture stress increased to a peak. The rupture force decreased to point c and increased again until the end of the compression (point d). Instead, the rupture stress deceased to point c and showed a slower decrease until point d. With this information as well as mathematic modeling [21], the rupture

displacement and rupture stress were obtained. As shown in Figure 3E, all microneedles ruptured at a displacement of around 10-20 μm. The loading of melittin significantly decreased the mechanical strength of the microneedles: melittin loading decreased the rupture stress of HA microneedles from 58 MPa to 38 MPa, while the loading into MeHA microneedles slightly decreased the rupture stress from 30 MPa to 27 MPa.

**Mel-HA-MN supressed RA progression in AIA rodent model**

We first studied the therapeutic potency of Mel-HA-MN in the rat AIA model. To investigate the penetration capacity of the microneedles, we applied the patch on the abdomen skin of rat, and the penetration efficiency was investigated with Trypan blue staining method. It was shown that the microneedles efficiently penetrated the skin (Figure 4A). To study the penetration depth of the microneedles, the holes made by the microneedles in the sectioned specimens of the penetrated skin were visualized by fluorescence microscopy. It was shown that Mel-HA-MN successfully pierced the skin with a penetration depth of around 200 μm. Additionally, melittin was successfully released inside the micro-holes made by microneedles after penetrating the skin for 3 min (Figure 4B).

Four days after induction of AIA, the microneedle patch was applied onto the animals every other day for 8 times and the therapeutic potency was evaluated by monitoring the body weight loss, change of paw thickness and clinical score of the symptoms (Figure 4C). As shown in Supplementary Figure 3, animals in all groups showed a similar weight loss percentage as compared to the base (Naive rats). Specifically, the weight loss percentage reached around 15% and stayed relatively stable until the end of the experiment. The paw thickness of model control rats increased by above 4 mm at the end of treatment (Figure 4D). By contrast, the paw thickness change of animals after receiving either S.C. injected melittin or Mel-HA-MN increased to around 2.5 mm on day 6, but started to decrease gradually to below 2 mm at the end of treatment, which was less than 50% of the thickness of model group. Similarly, melittin treatment by both S.C. and Mel-HA-MN groups decreased the clinical score by two-fold as compared to that in model control group (Figure 4D). The representative paw images further confirmed that the administration of melittin significantly stabilized the swelling of the paw and suppressed RA progression (Figure 4E).

Next, we checked the histology of the paws by H&E and Safranin O/fast green staining. The examination by H&E stain showed that the treatment of Mel-HA-MN or S.C. injection of melittin significantly preserved cartilage integrity and reduced the infiltration of leukocytes as compared to control group (a: cartilage destruction, b: leukocyte infiltration, indicated by arrows, Figure 4F). Safranin O/fast green staining showed similar trends as H&E staining that Mel-HA-MN and S.C. administered melittin effectively preserved the integrity of the cartilage, as indicated by the red stain of the chondrocytes. Hematologic parameters on day 22 were checked to examine the in vivo safety of our formulations. Results showed that control group significantly increased the WBC level as compared to naive rats (Figure 4G), probably due to the infection of Mycobacterium tuberculosis used for building the disease model [31]. Interestingly, S.C. injected and Mel-HA-MN mediated delivery of melittin reversed this trend. On the other hand, the treatment did not cause significant changes of RBC and PLT as compared to

naive animals. To sum, Mel-HA-MN effectively delivered melittin into rat skin and inhibited RA progression in AIA rodent model.

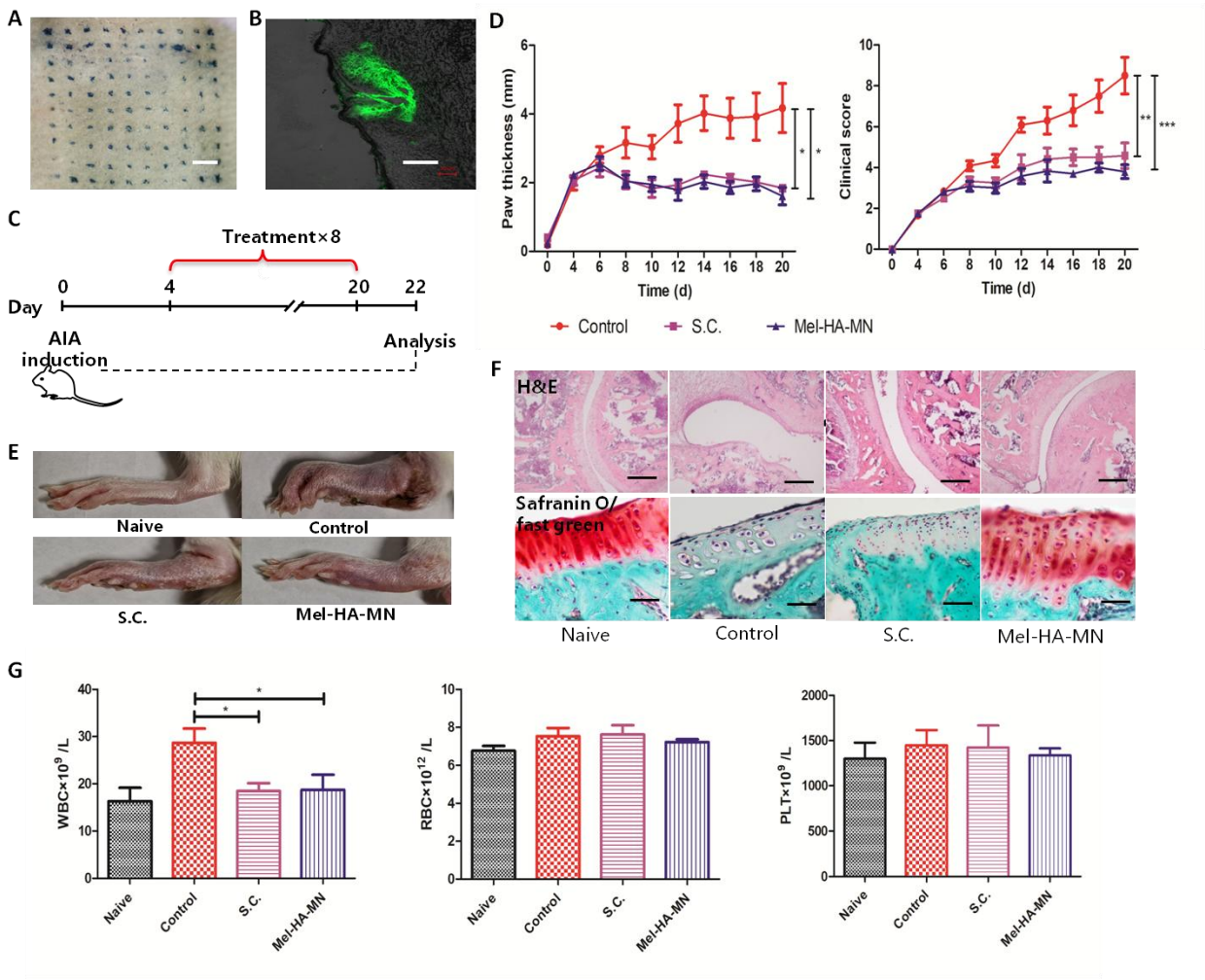


**Figure 4**. Therapeutic potency of Mel-HA-MN in rat AIA model. A: Penetrated skin stained by Trypan blue. Scale bar: 0.5 cm. B: Micro-channels made by Mel-HA-MN visualized by fluorescence microscopy. Scale bar: 100 μm. C: Experimental strategy for therapeutic potency study of the microneedle patch. D: Change of paw thickness and clinical score during treatment. E: Representative paw images of different treatment groups. F: H&E and Safranin O/fast green stain images of paws. a: cartilage destruction, b: cell infiltration. Scale bar: 1000 μm (upper) and 250 μm (lower). G. Hematologic parameters on day 22 including WBC, RBC and Platelets. Bars represent mean ± SEM, n = 6. *p<0.05, **p<0.01 and ***p<0.001.

**Mel-MeHA-MN significantly increased therapeutic efficacy in mouse AIA model**

Next, we investigated and compared therapeutic potency of Mel-MeHA-MN to Mel-HA-MN in AIA mouse model. Mice were administered with either Mel-HA-MN or Mel-MeHA-MN. The mice were treated every other day for 6 times with a melittin dose of 15 μg (Figure 5A).

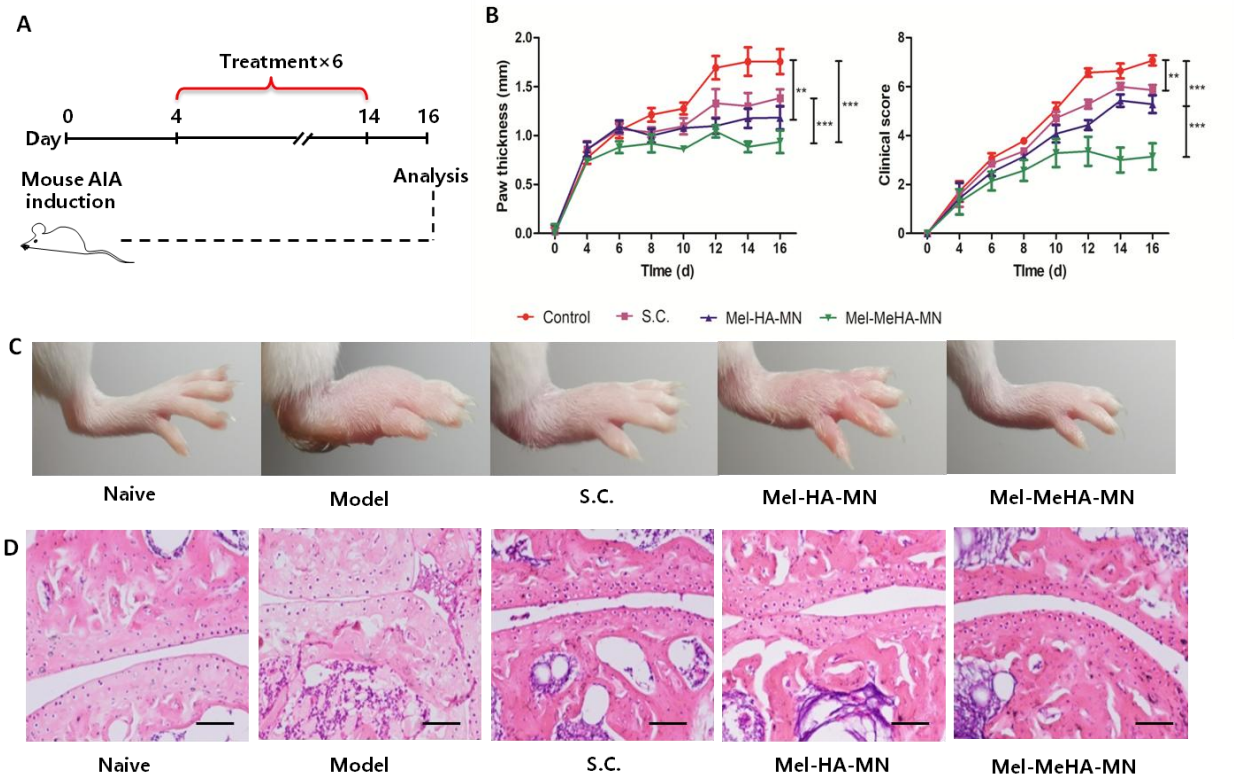


**Figure 5**. Therapeutic potency of Mel-MeHA-MN in mouse AIA model. A: Schematic diagram for studying therapeutic efficacy of Mel-MeHA-MN. B: Paw thickness change and clinical score during treatment. C: Representative images of paws from different groups. D: H&E staining of mice paws. Scale bar: 400 μm. Bars represent mean ± SEM, n = 6. *p<0.05, **p<0.01 and ***p<0.001.

The therapeutic potency of our fabricated microneedle systems in mice AIA was evaluated by monitoring weight loss, paw thickness change and clinical score. As shown in Supplementary Figure 4, the administration of melittin seemed to decrease weight loss percentage although the difference between the treated groups and control group was not significant. By the end of the study, the animals showed a weight loss percentage of 10-15% as compared to the base. As for paw thickness change, subcutaneous injection of melittin and Mel-HA-MN decreased the paw thickness by 20% and 30%, respectively, as compared to model control (Figure 5B). Importantly, Mel-MeHA-MN group reduced the paw thickness by a significantly larger level to 50%. The results of clinical score showed a similar trend: Mel-MeHA-MN group significantly decreased the clinical score as compared to model and S.C. groups (***p<0.001, Figure 5B).

Representative paw images further confirmed that the treatment by melittin effectively reduced the symptoms of the RA, including paw swelling and erythema (Figure 5C). Mel-MeHA-MN with a sustained release property of melittin showed a better protection efficacy as compared to S.C. group and Mel-HA-MN. H&E staining indicated that microneedle delivered melittin significantly reduced the infiltration of inflammatory cells and preserved the integrity of cartilages (Figure 5D). To sum, these results shown above indicated that the administration of sustained release microneedles could further improve RA therapeutic efficacy of melittin as compared to HA microneedles and S.C. injected melittin.

**Melittin loaded microneedles reduced levels of pro-inflammation cytokines and increased Treg cell percentages**

Next, we checked cytokine levels in the paws and blood serum to see if the application of melittin loaded microneedles inhibited RA progression by inhibiting expression of the pro-inflammation cytokines. We showed that TNF-α and IL-17 in both paws and serum were significantly decreased after the administration of melittin-loaded microneedles as compared to model control (Figure 6A-C). Specifically, Mel-MeHA-MN significantly decreased TNF-α levels in paws as compared to model control (***p<0.001, Figure 6A). Importantly, Mel-MeHA-MN also induced significantly lower level of TNF-α than both S.C. group and Mel-HA-MN group (*p<0.05). This trend was even more obvious for TNF-α in blood serum: microneedle-mediated delivery of melittin decreased TNF- α level by more than two times (Figure 6B). Mel-MeHA-MN showed a significantly stronger inhibition effect for TNF-α excretion than S.C. group. On the other hand, all groups after receiving melittin treatment significantly inhibited the level of IL-17 in paws by almost 3 times as compared to model control group. In this case, the difference between sustained release microneedle group and fast release microneedle and S.C. groups was not significant (Figure 6C).

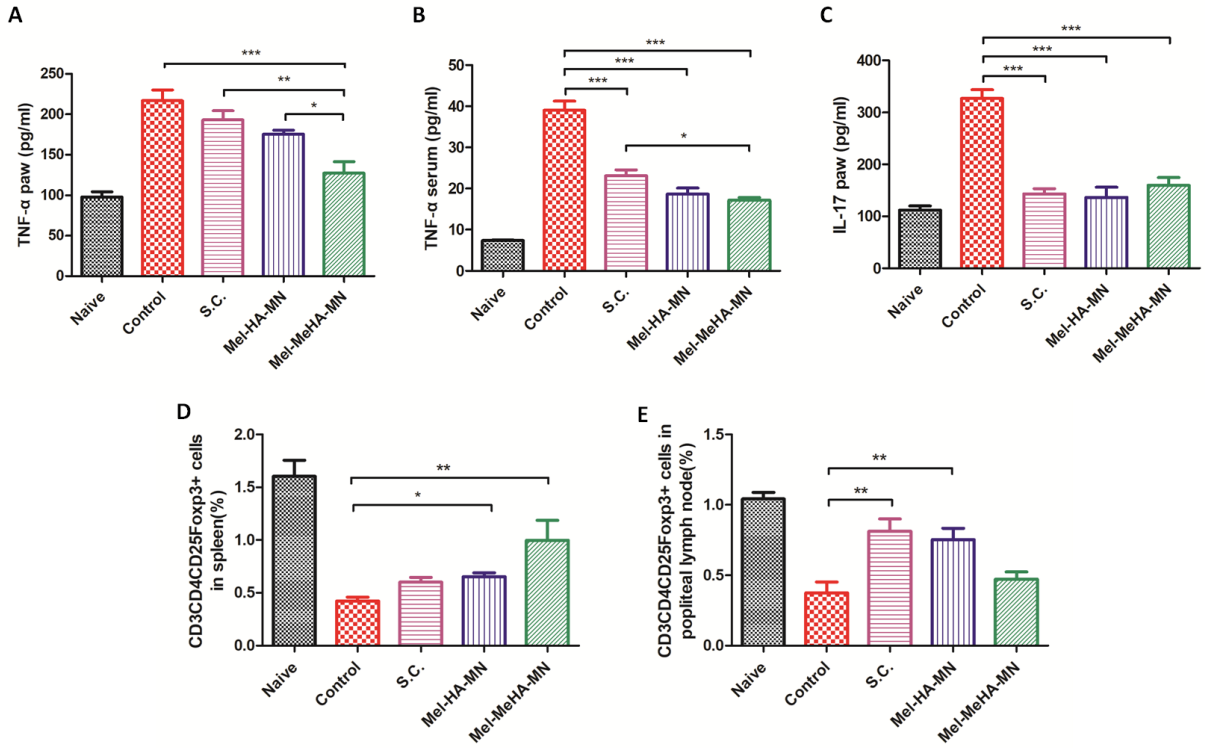


**Figure 6**. Cytokines and Treg cell percentages on day 16. A: Concentration of TNF-α in paws of mice. B: Concentration of TNF-α in blood serum. C: Concentration of IL-17 in paws. D: Percentage of Treg cells in spleen. E: Percentage of Treg cells in popliteal lymph node. Bars represent mean ± SEM, n = 6. *p<0.05, **p<0.01 and ***p<0.001.

We next checked Treg cell percentages in spleen and popliteal lymph nodes on day 16 by analyzing the percentage of $CD3CD4CD25Foxp3^{+}$ cells using flow cytometry. We observed that melittin delivered by

using microneedles significantly increased Treg cell percentage in spleen (Figure 6D). Additionally, the sustained release microneedle induced the highest level of Treg cells. As for Treg cells in popliteal lymph nodes, S.C. and HA-MN delivered melittin significantly increased the percentage of Treg cells as compared to model group (Figure 6E). Interestingly, the sustained release microneedle did not show any promotion of Treg cells in lymph nodes. These results above indicated that the microneedles may inhibit RA progression by inhibiting pro-inflammatory excretion and by increasing Treg cell percentages in lymphatic organs.

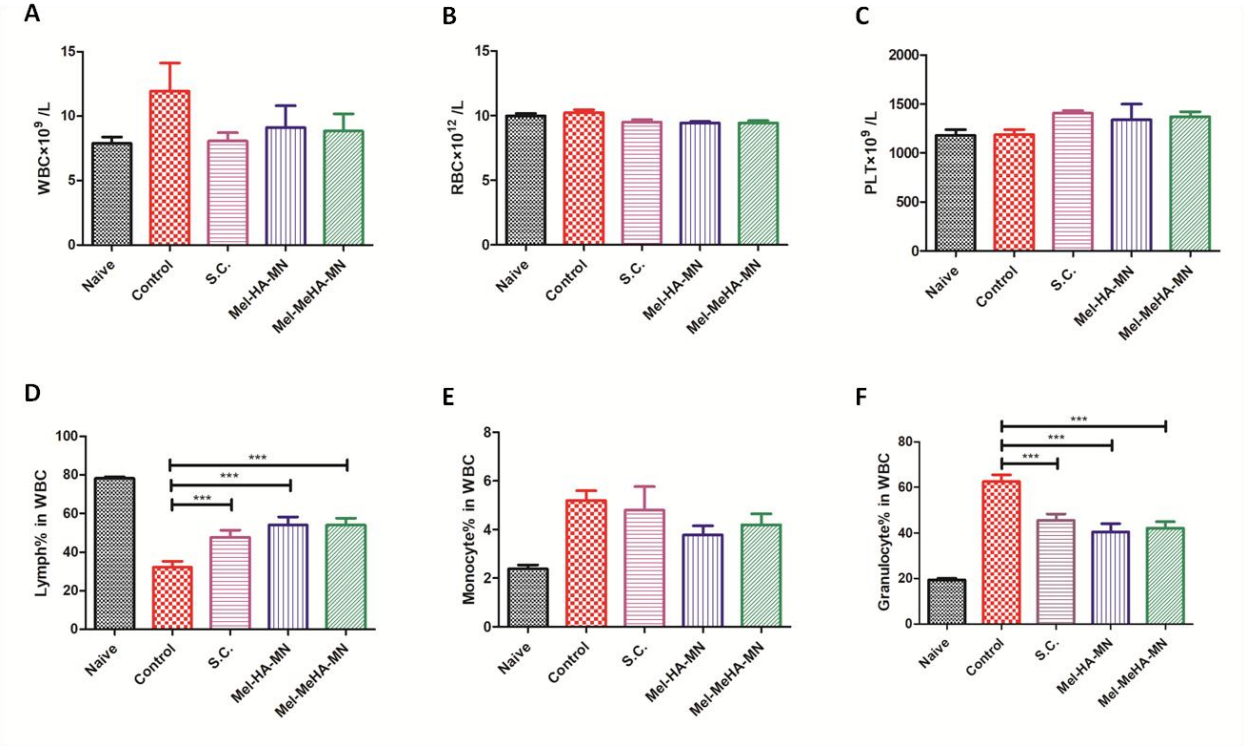


**Figure 7.** Hematologic parameters of microneedle-treated mice on day 16. A: White blood cell counts (WBC). B: Red blood cell counts (RBC). C: Platelets counts (PLT). D: Percentage of lymphcytes in WBC. E: Percentage of monocytes in WBC. F: Percentage of granulocytes in WBC. Bars represent mean ± SEM, n = 6. *p<0.05, **p<0.01 and ***p<0.001.

Finally, the hematologic parameters were checked to see if the treatment of melittin induced any blood cytotoxicity. Similar to the observation in rat AIA model, WBC counts were significantly increased in model control group, probably because of bacterial infection when building the RA disease model (Figure 7A). The use of melittin seemed to tune back this trend, although the difference between melittin treated groups and control group was not significant. The treatment by microneedles did not induce any significant change of RBC or PLT counts compared to naive mice (Figure 7B-C). Interestingly, control group showed significantly decreased percentage of lymphocytes, and increased percentages of monocytes and granulocytes as compared to naive cells, while the treatment by melittin loaded in microneedles effectively reversed this trend (Figure 7D-F).

## Discussion and conclusions

Transdermal drug delivery systems for RA therapy are attractive as they could overcome several drawbacks which exist in traditional strategies of oral uptake or injection of RA drugs, including low compliance, infection risk and low drug bioavailability. However, transdermal delivery efficiency of RA drugs especially for biological drugs is significantly limited due to the barrier function of stratum corneum in the skin. In this study, we fabricated HA-based polymeric microneedles for transdermal delivery of a peptide drug melittin, which is the main component for immune modulation and anti-RA effect in bee venom, aiming for increasing administration convenience and skin delivery efficiency. Our results showed that HA based microneedles could successfully overcome the skin barrier and deliver melittin into the skin. The delivered melittin was able to effectively inhibit the progression of RA and protect cartilage from being damaged, which was as effective as that induced by S.C. injection of melittin. More importantly, by simply modifying HA with cross-linkable groups, the fabricated microneedles could further increase the therapeutic efficacy. Our results revealed that microneedle based delivery system could provide an attractive trandermal RA therapy with improved patient compliance and therapeutic efficacy.

In this study, we first characterized the mechanical properties of individual polymeric microneedles by micromanipulation technique. The micromanipulation instrument was initially used to characterize the mechanical properties of individual cell and microparticles. In our previous study, we have extended its use for characterization of individual polymer microneedles and shown that the micromanipulation instrument is a very powerful tool for characterizing the mechanical properties of individual microneedles. We have also shown that rupture stress is a better indicator for mechanical properties of microneedles as compared to rupture force, as rupture stress can be regarded as an intrinsic material property parameter of microneedles [21]. In the current study, we found that the loading of drug could significantly decrease the rupture stress of the corresponding microneedles, which is similar to what we observed in the last study. The mean ultimate rupture strength of human skin was reported to be 27.2 ± 9.3 MPa [32]. All the mean values of the obtained rupture stress of the microneedle patches in this work are not less than this value, indicating that these microneedles may be strong enough to pierce the human skin and our microneedles could have potential for future clinical use. Nevertheless, we showed that our fabricated microneedles were strong enough to pierce and to deliver the loaded melittin into the skin.

Traditional polymer based dissolving microneedles normally have a fast drug-dissolving rate after being inserted into the skin [33, 34]. Recent research put a lot of efforts on developing microneedles with controlled release properties of the loaded drugs, aiming for improving drug efficacy and reducing side effects [14, 35]. We here fabricated melittin-loaded HA microneedles with slow-release properties by simply modifying the polymer with cross-linkable groups. Our results showed that as compared to Mel-HA-MN with fast release properties, the prepared Mel-MeHA-MN possessed improved therapeutic capacity on inhibiting RA symptoms. Cytokine and cell immunity study revealed that the sustained release microneedles could further decrease the levels of pro-inflammatory cytokines and increase the Treg cell percentages. The observed advantages of sustained release microneedles were consistent with previous findings that sustained release of drug or vaccine from microneedles could increase drug efficacy or vaccine immunogenicity [17, 36-38]. For example, Gu et al. showed that MeHA based

microneedles could sustainedly release the loaded insulin, and as a result could better control blood glucose level and improve the safety of insulin delivery [28, 39]. In another study, chitosan microneedles loaded with a model antigen OVA elicited superior immune responses which lasted for more than 6 weeks after only one dose [40]. The improved therapeutic efficacy against RA by sustained release of drug found in the current study is also consistent with our findings in previous research. For instance, we have previously shown that after intravenous injection of polymeric micelles with sustained release property of dexamethasone, the drug accumulation in the inflammatory joint was significantly increased and their inhibition potency of RA was robustly enhanced [41-43]. In summary, our current study indicates that microneedle based delivery system could be an alternative strategy for sustained delivery of RA drug to improve RA drug efficacy.

Herein, we chose a peptide drug melittin to investigate the delivery capacity of our fabricate microneedles. Previous studies have shown that melittin could inhibit RA progression by inhibiting the excretion of pro-inflammatory cytokines after interacting with NF-KB pathway [44]. In our current study, we indeed showed that microneedle-mediated delivery of melittin could inhibit expression of TNF-α and IL-17 in both paws and blood serum. Additionally, we observed that the application of melittin could increase Treg cell amount in lymphatic organs including spleen and popliteal lymph nodes. RA is an autoimmune disease caused by the loss of self-tolerance while regulatory $CD4^+$ T cells play a key role in maintaining self-tolerance [45]. Although the mechanism of melittin to increase Treg cell amount remains to be explored, our results indicated that microneedle-mediated delivery of melittin could have potential for tuning of T cell imbalances in autoimmune diseases [46, 47].

Bee venom acupuncture has been used for the treatment of RA for a long time [48, 49]. However, the significant pain sensation and requirement on live bees have significantly limited the application of this strategy. Our results showed that microneedle-mediated melittin delivery could have potential to improve this method. Specifically, microneedle strategies have advantages including easiness for administration and potential for improving the stability of the loaded drug. Polymeric microneedles also allow controlled drug release to improve drug therapeutic efficacy by polymer modification. Additionally, although melittin has a risk to cause hemolysis due to their strong cell membrane penetrating function [27, 50, 51], our results showed that the administration of melittin did not cause significant blood cytotoxicity. Biodistribution results indicated that this could be caused by the fact that the blood concentration of melittin was much lower than its hemolytic concentration (Supplementary Figure 2).

Finally, the relative low drug loading capacity of microneedles is one important factor limiting their possible clinical translation. The amplification of loaded drug amount from the level for experiment animal models to human is still a challenge lying in front before microneedles can be applied to patients. In our current study, we investigated the therapeutic efficacy of sustained release microneedles in mice model, partly due to the fact that our fabricated microneedles could easily fulfill sustainedly releasing therapeutic relevant dose for mice. Nevertheless, recent studies have tried to solve this obstacle by further enlarging the size of the microneedle patch or by utilizing new fabrication strategies to increase maximum loading capacity in a single patch [36, 52]. For instance, Yu et al. increased loading amount of insulin in a patch by increasing the patch size to 5 $cm^2$. They showed that the enlarged patch could deliver insulin for controlling glucose level in a minipig model with a weight of 25 kg. It was shown that

one microneedle patch could effectively release enough insulin for glucose level regulation within a time period of more than 20 h [17]. In another study, Tran et al. fabricated core-shell microneedles in which the microneedle core was filled with drug suspension or powder to increase drug loading amount. The fabricated microneedles showed a programmed release property of multi-drugs and can release the drugs from a few days to more than a month after a single administration [52]. These new strategies for increasing loading capacity of microneedles could help to promote the translation of microneedle technology.

In conclusion, our study showed that polymeric microneedles is a promising transdermal delivery strategy for melittin to improve treatment of RA, by enhancing administration convenience and by modulating release properties of the loaded drug. The sustained release of melittin showed potential to further increase therapeutic efficacy and reduce administration frequency. This study has laid foundation for designing non-invasive and highly potent treatment strategy for RA and other autoimmune diseases.

**Acknowledgements**

We acknowledge the financial support of the National Natural Science Foundation of China (No. 81961130395, No. 82003684), China Postdoctoral Science Foundation Grant (2019M663534), Program of Introducing Talents of Discipline to Universities (Plan 111, No. B18035), and NAF\R1\191217 - Newton Advanced Fellowships 2019.

**Conflict of interest:** There is no conflict of interest.

**References:**

[1] J.S. Smolen, D. Aletaha, I.B. McInnes, Rheumatoid arthritis, The Lancet, 388 (2016) 2023-2038.
[2] B. Combe, R. Landewe, C.I. Daien, C. Hua, D. Aletaha, J.M. Álvaro-Gracia, M. Bakkers, N. Brodin, G.R. Burmester, C. Codreanu, R. Conway, M. Dougados, P. Emery, G. Ferraccioli, J. Fonseca, K. Raza, L. Silva-Fernández, J.S. Smolen, D. Skingle, Z. Szekanecz, T.K. Kvien, A. van der Helm-van Mil, R. van Vollenhoven, 2016 update of the EULAR recommendations for the management of early arthritis, Ann Rheum Dis, 76 (2017) 948-959.
[3] D. Aletaha, J.S. Smolen, Diagnosis and Management of Rheumatoid Arthritis: A Review, Jama, 320 (2018) 1360-1372.
[4] W. Wang, H. Zhou, L. Liu, Side effects of methotrexate therapy for rheumatoid arthritis: A systematic review, European journal of medicinal chemistry, 158 (2018) 502-516.
[5] E. Moroz, S. Matoori, J.C. Leroux, Oral delivery of macromolecular drugs: Where we are after almost 100years of attempts, Advanced drug delivery reviews, 101 (2016) 108-121.
[6] M. Qindeel, M.H. Ullah, D. Fakhar ud, N. Ahmed, A.u. Rehman, Recent trends, challenges and future outlook of transdermal drug delivery systems for rheumatoid arthritis therapy, Journal of Controlled Release, 327 (2020) 595-615.
[7] P. Wu, Q. Liang, P. Feng, C. Li, C. Yang, H. Liang, H. Tang, C. Shuai, A Novel Brucine Gel Transdermal Delivery System Designed for Anti-Inflammatory and Analgesic Activities, International journal of molecular sciences, 18 (2017).
[8] S.F. Ng, L.S. Tan, F. Buang, Transdermal anti-inflammatory activity of bilayer film containing olive compound hydroxytyrosol: physical assessment, in vivo dermal safety and efficacy study in Freund's adjuvant-induced arthritic rat model, Drug development and industrial pharmacy, 43 (2017) 108-119.

[9] M. Lodzki, B. Godin, L. Rakou, R. Mechoulam, R. Gallily, E. Touitou, Cannabidiol-transdermal delivery and anti-inflammatory effect in a murine model, Journal of controlled release : official journal of the Controlled Release Society, 93 (2003) 377-387.
[10] Y. Gu, X. Tang, M. Yang, D. Yang, J. Liu, Transdermal drug delivery of triptolide-loaded nanostructured lipid carriers: Preparation, pharmacokinetic, and evaluation for rheumatoid arthritis, International Journal of Pharmaceutics, 554 (2019) 235-244.
[11] Q.D. Pham, S. Björklund, J. Engblom, D. Topgaard, E. Sparr, Chemical penetration enhancers in stratum corneum - Relation between molecular effects and barrier function, Journal of controlled release : official journal of the Controlled Release Society, 232 (2016) 175-187.
[12] K. Ita, Transdermal Delivery of Drugs with Microneedles-Potential and Challenges, Pharmaceutics, 7 (2015) 90-105.
[13] Y.-C. Kim, J.-H. Park, M.R. Prausnitz, Microneedles for drug and vaccine delivery, Advanced drug delivery reviews, 64 (2012) 1547-1568.
[14] G. Du, X. Sun, Current Advances in Sustained Release Microneedles, Pharmaceutical Fronts, 02 (2020) e11-e22.
[15] M. Kirkby, A.R.J. Hutton, R.F. Donnelly, Microneedle Mediated Transdermal Delivery of Protein, Peptide and Antibody Based Therapeutics: Current Status and Future Considerations, Nature Public Health Emergency Collection, 37.
[16] Y. Ye, C. Wang, X. Zhang, Q. Hu, Y. Zhang, Q. Liu, D. Wen, J. Milligan, A. Bellotti, L. Huang, G. Dotti, Z. Gu, A melanin-mediated cancer immunotherapy patch, Science Immunology, 2 (2017) eaan5692.
[17] J. Yu, J. Wang, Y. Zhang, G. Chen, W. Mao, Y. Ye, A.R. Kahkoska, J.B. Buse, R. Langer, Z. Gu, Glucose-responsive insulin patch for the regulation of blood glucose in mice and minipigs, Nature Biomedical Engineering, 4 (2020) 499-506.
[18] S.D. Gittard, B. Chen, H. Xu, A. Ovsianikov, B.N. Chichkov, N.A. Monteiro-Riviere, R.J. Narayan, The Effects of Geometry on Skin Penetration and Failure of Polymer Microneedles, Journal of Adhesion Science & Technology, 27 (2013) 227-243.
[19] J.H. Park, M.R. Prausnitz, Analysis of Mechanical Failure of Polymer Microneedles by Axial Force, The journal of the Korean Physical Society, 56 (2010) 1223-1227.
[20] J.H. Park, M.G. Allen, M.R. Prausnitz, Polymer microneedles for controlled-release drug delivery, Pharmaceutical research, 23 (2006) 1008-1019.
[21] G. Du, Z. Zhang, P. He, Z. Zhang, X. Sun, Determination of the mechanical properties of polymeric microneedles by micromanipulation, Journal of the mechanical behavior of biomedical materials, 117 (2021) 104384.
[22] B.V. Nguyen, Q.G. Wang, N.J. Kuiper, A.J. El Haj, C.R. Thomas, Z. Zhang, Biomechanical properties of single chondrocytes and chondrons determined by micromanipulation and finite-element modelling, Journal of the Royal Society, Interface, 7 (2010) 1723-1733.
[23] J.-D. Lee, H.-J. Park, Y. Chae, S. Lim, An Overview of Bee Venom Acupuncture in the Treatment of Arthritis, Evid Based Complement Alternat Med, 2 (2005) 79-84.
[24] Y.B. Kwon, H.J. Lee, H.J. Han, W.C. Mar, S.K. Kang, O.B. Yoon, A.J. Beitz, J.H. Lee, The water-soluble fraction of bee venom produces antinociceptive and anti-inflammatory effects on rheumatoid arthritis in rats, Life Sciences, 71 (2002) 191-204.
[25] S.-J. Hong, G.S. Rim, H.I. Yang, C.S. Yin, H.G. Koh, M.-H. Jang, C.-J. Kim, B.-K. Choe, J.-H. Chung, Bee venom induces apoptosis through caspase-3 activation in synovial fibroblasts of patients with rheumatoid arthritis, Toxicon, 46 (2005) 39-45.
[26] Bae, Hyunsu, Lee, Gihyun, Anti-Inflammatory Applications of Melittin, a Major Component of Bee Venom: Detailed Mechanism of Action and Adverse Effects, Molecules, (2016).
[27] W.F. DeGrado, G.F. Musso, M. Lieber, E.T. Kaiser, F.J. Kézdy, Kinetics and mechanism of hemolysis induced by melittin and by a synthetic melittin analogue, Biophysical journal, 37 (1982) 329-338.

[28] Y.Q. Ye, J.C. Yu, C. Wang, N.Y. Nguyen, G.M. Walker, J.B. Buse, Z. Gu, Microneedles Integrated with Pancreatic Cells and Synthetic Glucose-Signal Amplifiers for Smart Insulin Delivery, Adv Mater, 28 (2016) 3115-3121.
[29] Li, Jinghua, Ke, Tao, He, Chao, C. o, Wei, Mengqi, Zhang, The Anti-Arthritic Effects of Synthetic Melittin on the Complete Freund's Adjuvant-Induced Rheumatoid Arthritis Model in Rats, American Journal of Chinese Medicine, (2010).
[30] J.D. Lee, S.Y. Kim, T.W. Kim, S.H. Lee, H.I. Yang, D.I. Lee, Y.H. Lee, Anti-inflammatory effect of bee venom on type II collagen-induced arthritis, The American journal of Chinese medicine, 32 (2004) 361-367.
[31] H.J. Mahdi, N.A.K. Khan, M.Z.B. Asmawi, R. Mahmud, A.L.M. V, In vivo anti-arthritic and anti-nociceptive effects of ethanol extract of Moringa oleifera leaves on complete Freund's adjuvant (CFA)-induced arthritis in rats, Integrative medicine research, 7 (2018) 85-94.
[32] A.J. Gallagher, A.N. Annaidh, K. Bruyère, et al., Dynamic Tensile Properties of Human Skin, in, International Research Council on the Biomechanics of Injury, 2012.
[33] J.W. Lee, J.H. Park, M.R. Prausnitz, Dissolving microneedles for transdermal drug delivery, Biomaterials, 29 (2008) 2113-2124.
[34] K. Ita, Dissolving microneedles for transdermal drug delivery: Advances and challenges, Biomedicine & Pharmacotherapy, 93 (2017) 1116-1127.
[35] P. Singh, A. Carrier, Y. Chen, S. Lin, X. Zhang, Polymeric microneedles for controlled transdermal drug delivery, Journal of Controlled Release, 315 (2019) 97-113.
[36] S. Kim, H. Yang, J. Eum, Y. Ma, S. Fakhraei Lahiji, H. Jung, Implantable powder-carrying microneedles for transdermal delivery of high-dose insulin with enhanced activity, Biomaterials, 232 (2020) 119733.
[37] J. Yu, Y. Zhang, Z. Gu, Glucose-Responsive Insulin Delivery by Microneedle-Array Patches Loaded with Hypoxia-Sensitive Vesicles, Methods Mol Biol, 1570 (2017) 251-259.
[38] P.C. Demuth, J.J. Moon, H. Suh, P.T. Hammond, D.J. Irvine, Releasable Layer-by-Layer Assembly of Stabilized Lipid Nanocapsules on Microneedles for Enhanced Transcutaneous Vaccine Delivery, Acs Nano, 6 (2012) 8041.
[39] J. Di, S. Yao, Y. Ye, Z. Cui, J. Yu, T.K. Ghosh, Y. Zhu, Z. Gu, Stretch-Triggered Drug Delivery from Wearable Elastomer Films Containing Therapeutic Depots, ACS Nano, 9 (2015) 9407-9415.
[40] M.C. Chen, S.F. Huang, K.Y. Lai, M.H. Ling, Fully embeddable chitosan microneedles as a sustained release depot for intradermal vaccination, Biomaterials, 34 (2013) 3077-3086.
[41] Q. Wang, J. Jiang, W. Chen, H. Jiang, Z. Zhang, X. Sun, Targeted delivery of low-dose dexamethasone using PCL–PEG micelles for effective treatment of rheumatoid arthritis, Journal of Controlled Release, 230 (2016) 64-72.
[42] Q. Wang, Y. Li, X. Chen, H. Jiang, Z. Zhang, X. Sun, Optimized in vivo performance of acid-liable micelles for the treatment of rheumatoid arthritis by one single injection, Nano research, (2019).
[43] Q. Wang, H. Jiang, Y. Li, W. Chen, H. Li, K. Peng, Z. Zhang, X. Sun, Targeting NF-kB signaling with polymeric hybrid micelles that co-deliver siRNA and dexamethasone for arthritis therapy, Biomaterials, 122 (2017) 10-22.
[44] H.J. Park, S.H. Lee, D.J. Son, K.W. Oh, K.H. Kim, H.S. Song, G.J. Kim, G.T. Oh, D.Y. Yoon, J.T. Hong, Antiarthritic effect of bee venom: inhibition of inflammation mediator generation by suppression of NF-kappaB through interaction with the p50 subunit, Arthritis and rheumatism, 50 (2004) 3504-3515.
[45] F.A.H. Cooles, J.D. Isaacs, A.E. Anderson, Treg Cells in Rheumatoid Arthritis: An Update, Current Rheumatology Reports, 15 (2013) 352.
[46] J. Li, T. Ke, C. He, W. Cao, M. Wei, L. Zhang, J.-X. Zhang, W. Wang, J. Ma, Z.-R. Wang, Z.-J. Shao, The Anti-Arthritic Effects of Synthetic Melittin on the Complete Freund's Adjuvant-Induced Rheumatoid Arthritis Model in Rats, The American Journal of Chinese Medicine, 38 (2010) 1039-1049.

[47] G. Lee, H. Bae, Anti-Inflammatory Applications of Melittin, a Major Component of Bee Venom: Detailed Mechanism of Action and Adverse Effects, Molecules, 21 (2016) 616.
[48] J.A. Lee, M.J. Son, J. Choi, J.H. Jun, J.-I. Kim, M.S. Lee, Bee venom acupuncture for rheumatoid arthritis: a systematic review of randomised clinical trials, BMJ Open, 4 (2014) e006140.
[49] X. Chen, H. Fan, J. Chen, H. Fan, P. Wu, Bee venom acupuncture for adhesive capsulitis: A protocol for systematic review and meta-analysis, Medicine, 99 (2020).
[50] M.T. Tosteson, S.J. Holmes, M. Razin, D.C. Tosteson, Melittin lysis of red cells, The Journal of membrane biology, 87 (1985) 35-44.
[51] H. Zarrinnahad, A. Mahmoodzadeh, M.P. Hamidi, M. Mahdavi, A. Moradi, K.P. Bagheri, D. Shahbazzadeh, Apoptotic Effect of Melittin Purified from Iranian Honey Bee Venom on Human Cervical Cancer HeLa Cell Line, International Journal of Peptide Research and Therapeutics, 24 (2018) 563-570.
[52] K.T.M. Tran, T.D. Gavitt, N.J. Farrell, E.J. Curry, A.B. Mara, A. Patel, L. Brown, S. Kilpatrick, R. Piotrowska, N. Mishra, S.M. Szczepanek, T.D. Nguyen, Transdermal microneedles for the programmable burst release of multiple vaccine payloads, Nature Biomedical Engineering, (2020).